Mathematical model to analyze the dissolution behavior of metastable crystals or amorphous drug accompanied with a solid-liquid interface reaction

Daiki Hirai, Yasunori Iwao, Shin-ichiro Kimura, Shuji Noguchi, Shigeru Itai*

Department of Pharmaceutical Engineering and Drug Delivery Science, School of Pharmaceutical Sciences, University of Shizuoka. 52-1 Yada, Suruga-ku, Shizuoka, 422-8526, Japan.

*Corresponding author. E-mail: s-itai@u-shizuoka-ken.ac.jp; Tel.: +81-54-264-5614; Fax: +81-54-264-5615.

12

table of contents graphic

Hirai *et al.*

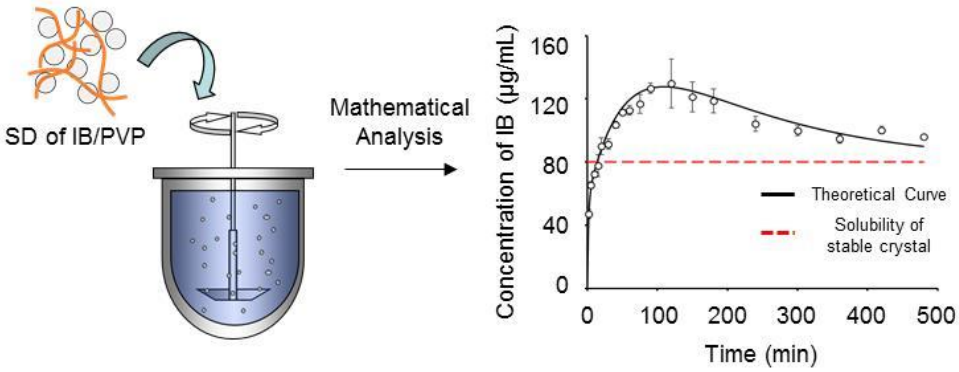

13

ABSTRACT

Metastable crystals and the amorphous state of poorly water-soluble drugs in solid dispersions (SDs), are subject to a solid-liquid interface reaction upon exposure to a solvent. The dissolution behavior during the solid-liquid interface reaction often shows that the concentration of drugs is supersaturated, with a high initial drug concentration compared with the solubility of stable crystals but finally approaching the latter solubility with time. However, a method for measuring the precipitation rate of stable crystals and/or the potential solubility of metastable crystals or amorphous drugs has not been established. In this study, a novel mathematical model that can represent the dissolution behavior of the solid-liquid interface reaction for metastable crystals or amorphous drug was developed and its validity was evaluated. The theory for this model was based on the Noyes-Whitney equation and assumes that the precipitation of stable crystals at the solid-liquid interface occurs through a first-order reaction. Moreover, two models were developed, one assuming that the surface area of the drug remains constant because of the presence of excess drug in the bulk and the other that the surface area changes in time-dependency because of agglomeration of the drug. SDs of Ibuprofen (IB) / polyvinylpyrrolidone (PVP) were prepared and their dissolution behaviors under non-sink conditions were fitted by the models to evaluate improvements in solubility. The model assuming time-dependent surface area showed good agreement with experimental values. Furthermore, by applying the model to the dissolution profile, parameters such as the precipitation rate and the potential solubility of the amorphous drug were successfully calculated. In addition, it was shown that the improvement in solubility with supersaturation was able to be evaluated quantitatively using this model. Therefore, this mathematical model would be a useful tool to quantitatively determine the supersaturation concentration of a metastable drug from solid dispersions.

KEYWORDS: Solid dispersions, solid-liquid interfaces, supersaturation, mathematical model, dissolution, agglomeration, ibuprofen, polyvinylpyrrolidone.

1. Introduction

In past few decades, most pharmaceutical products and candidates have had poor water solubility (Kawabata et al., 2011), and various techniques have been used to solve this disadvantage, including formulation as polymorphs (Paaver et al., 2012), amorphous (Nielsen et al., 2015), co-crystals (Sanphui et al., 2015), nanosuspensions (Douroumis and Fahr, 2006), and lipid nanoparticles (Makwana et al., 2015). Of these, the solid dispersion (SD), which can maintain the metastable crystal and amorphous state of compounds through specific interactions with polymers (Mishra et al., 2015; Dukeck et al., 2013), is widely applied to various drugs to improve solubility and subsequently enhance oral absorption. In general, solubilized drugs are in a supersaturated state, with a high drug concentration compared with the solubility of stable crystals and the dissolution behavior of the drug in the supersaturated state tends to achieve a stable plateau with the precipitation of stable crystals (Wlodarski et al., 2015; Knopp et al., 2016; Sarode et al., 2013). The rate of precipitation to form stable crystals and/or the degree of maintenance in the supersaturation state depend on the interactions between the drugs and the polymers (Sarode et al., 2014; Jackson et al., 2016; Ozaki et al., 2013; Mah et al., 2016). Therefore, quantitative evaluation of these interactions would enable the development of formulations with improved solubility. However, it is extremely difficult to directly measure and determine the potential solubility of metastable crystals and amorphous forms during dissolution studies.

One approach to determining the dissolution behavior of a drug is through the use of a mathematical model that can describe physical phenomena such as dissolution processes. Such a mathematical model has the advantage of reducing the number of experiments required to determine the mechanism of drug dissolution from a formulation. The “Noyes-Whitney” dissolution rate equation is a formula that describes the dissolution behavior of a solid preparation (Noyes and Whitney, 1897). In addition, the simulation of the dissolution

process and the prediction of oral absorption using mathematical models have also been attempted and is a useful tool for understanding mechanisms derived from internal changes in the drug (Sugano, 2011; Jakubiak et al., 2016; Chen et al., 2016; Tsume et al., 2015).

Recently, various models have been applied to the dissolution process of metastable crystals and amorphous drug at the solid-liquid interface. Laaksonen and Aaltonen attempted to develop a model that would express the change in drug crystal transition from the surface of a crystal in metastasis under the sink condition (Laaksonen and Aaltonen, 2013); however, use of the sink condition meant they were unable to analyze the dissolution profile of a supersaturated drug. Conversely, Sun and Lee modeled dissolution from the amorphous drug to a supersaturated state under a non-sink condition, and successfully determined the rate constant for reaching supersaturation, and the precipitation rate of stable crystals (Sun and Lee, 2013). However, the system of equations involved is too complex and predicted values over-estimated the time required for precipitation compared with experimental measurements. In addition, Gao described an integrated model of dissolution kinetics for a solute whose concentration at the solid-liquid interface changes with time, based on the Noyes-Whitney Equation (Gao, 2012). In Gao's model, it was assumed that the solvation or precipitation reaction could be approximated by a first-order reaction occurring at the solid-liquid interface, with the concentration gradient in the diffusion layer changing with time and the diffusional flux following Fick's law (i.e. proportional to the concentration gradient). It was also assumed that the surface area of the solute did not change so that the rate constant was treated as time-independent. As a result, the model suggested potential for the analysis of parameters related to the dissolution of the drug that trigger interfacial reactions such as the rate of precipitation of stable crystals. However, even in this model, it is difficult to analyze the potential solubility of a metastable crystal or amorphous form before precipitation of stable crystals and to quantitatively evaluate supersaturation. Because the

concentration of a supersaturated drug is maintained at a high level for long periods, the blood concentration of the drug and the area under the concentration-time curve (AUC) might also become high (Childs et al., 2013; Knopp et al., 2016; Zhang et al., 2016). Therefore, comprehensive and quantitative evaluation of supersaturation can be useful *in vitro* for the predicting improvements in drug concentrations *in vivo.*

In this study, we focused on the diffusion process at the solid-liquid interface and attempted to derive and evaluate a novel macroscopic mathematical model that describes the dissolution process of a drug with an interface reaction such as between metastable crystals and the amorphous drug under non-sink conditions. To measure the dissolution profile of an amorphous drug, a SD of Ibuprofen (IB) and polyvinylpyrrolidone (PVP), which is a combination often used for solubilization studies, was prepared by the solvent method (Najib at al., 1986; Rami-Abraham et al., 2015). We successfully developed two models with a constant surface area by adding excess drug and with a surface area that changed with time, and tried to evaluate their respective dissolution kinetics without using a rotating disk. In addition, using this model, the potential solubility of amorphous drugs in SD was quantitatively estimated and related to the preservation of supersaturation.

2. Theoretical basis

2.1. The case in which surface area is constant

The Noyes-Whitney equation is generally known to describe the diffusion process of a drug with a diffusion-controlling dissolution profile (Sarode et al., 2013). The dissolution model under this condition is shown in **Figure 1A** and the equation used to describe the dissolution process is given by

$$\frac{\mathrm{d}C_{\mathrm{b}}}{\mathrm{d}t} = \frac{kS}{V}\left(C_{\mathrm{S}} - C_{\mathrm{b}}\right), \tag{1}$$

where C_{b} represents the concentration of a drug in the system as a function of time t, S is the surface area of the drug, V is the volume of the medium, and C_{S} is the solubility of the drug. Furthermore, k represents the dissolution rate constant, defined as $k = D/h$, if D is the diffusion coefficient and h is the thickness of the diffusion layer. Solving Eq. (1) for C_{b}, gives

$$C_{\mathrm{b}} = C_{\mathrm{S}}\left\{1 - \exp\left(-\frac{kS}{V}t\right)\right\}. \tag{2}$$

Conversely, the dissolution model for a drug with a solid-liquid interface reaction is shown in **Figure 1B**. Here, C_{M} denotes the solubility of metastable crystals or amorphous drug and C_{S} is the solubility of stable crystals. In this study, the change in concentration of the drug at the solid-liquid interface was modeled on the basis of the theory described by Gao (Gao, 2012), in which it is assumed that the concentration of the drug at the interface changes with time and can be approximated using a first-order reaction. The concentration of the drug at the solid-liquid interface is regarded as a function of time, $C_{\mathrm{SL}}(t)$. At $t = 0$, the concentration of the drug at the solid-liquid interface equals the solubility of metastable crystals or amorphous drug, so

$$C_{\mathrm{SL}}(0) = C_{\mathrm{M}}. \tag{3}$$

However, the concentration of the drug at the solid-liquid interface gradually decreases because stable crystals precipitate with time through exposure to the medium.

Finally, the concentration reaches the concentration of stable crystals and the dissolution process terminates. If the crystal precipitation reaction follow a first-order proportionality and the crystal precipitation rate is defined as k_C, $C_{SL}(t)$ is assumed as follows,

$$\frac{dC_{SL}(t)}{dt} = k_C(C_S - C_{SL}(t)). \quad (4)$$

This equation can be solved to give

$$C_{SL}(t) = C_S - (C_M - C_S)\exp(-k_C t). \quad (5)$$

Furthermore, if it is assumed that the change with time in drug concentration is proportional to the concentration gradient across the diffusion layer, the dissolution rate equation with a solid-liquid interface reaction is given by

$$\frac{dC_b}{dt} = \frac{kS}{V}(C_{SL}(t) - C_b), \quad (6)$$

where the surface area of the drug varies during dissolution in the solution, so S is not regarded to be constant but is represented by an arbitrary function of time, $\sigma(t)$. Therefore, Eq. (6) can be expressed as

$$\frac{dC_b}{dt} = \frac{k\sigma(t)}{V}(C_{SL}(t) - C_b). \quad (7)$$

In the case of drug particles that are metastable crystals or amorphous, $\sigma(t)$ decreases with dissolution of the drug but increases with the precipitation of stable crystals. However, when a drug is studied using a rotating disk or is in excess, changes in surface area caused by dissolution can be regarded as very small and constant, and therefore neglected (Dokoumetzidis and Macheras, 2006; Tsinman et al., 2009). In this case, the term kS/V in Eq. (6) is constant and Eq. (6) is transformed to

$$\frac{dC_b}{dt} = k_D(C_{SL}(t) - C_b), \quad (8)$$

where, k_D is a constant that satisfies $k_D = kS/V$ and is defined as the dissolution rate constant. Eq. (5) is incorporated into Eq. (8) to give Eq. (9) as follows:

$$\frac{dC_b}{dt} = k_D\{C_S - (C_M - C_S)\exp(-k_C t) - C_b\}. \quad (9)$$

Solving Eq. (9) for C_b give the following relation:

$$C_b = C_S\{1 - \exp(-k_D t)\} + \frac{k_D(C_M - C_S)}{k_D - k_C}\{\exp(-k_C t) - \exp(-k_D t)\} \quad (10)$$

In Eqs. (2) and (10), when C_b is plotted versus t as shown in **Figure 2**, C_{max} is the maximum drug concentration and T_{max} is the time needed to reach C_{max}. The area Y surrounded by the curves from Eq. (2) (line A) and Eq. (10) (line B) expresses the increment in the dissolution with supersaturation and Y is thought to represent an index for the comprehensive evaluation of supersaturation. This parameter can be calculated by rearranging the model equations. The increment of Y in dissolution is thus given by

$$Y = \int_0^\infty \left[C_S\{1 - \exp(-k_D t)\} + \frac{k_D(C_M - C_S)}{k_D - k_C}\{\exp(-k_C t) - \exp(-k_D t)\} - C_S\left\{1 - \exp\left(-\frac{kS}{V}t\right)\right\}\right] dt, \quad (11)$$

Taking $k_D = kS/V$ into consideration, solving Eq. (11) gives

$$Y = \frac{C_M - C_S}{k_C}. \quad (12)$$

When the concentration of the drug reaches the maximum, $dC_b/dt = 0$. Calculating dC_b/dt gives

$$\frac{dC_b}{dt} = k_D C_S \exp(-k_D t) + \frac{k_D(C_M - C_S)}{k_D - k_C}\{-k_C \exp(-k_C t) + k_D \exp(-k_D t)\}. \quad (13)$$

If the right hand side of Eq. (13) equals 0, the solution for t gives T_{max}, given by

$$T_{max} = \frac{1}{k_D - k_C}\ln\left\{\frac{k_D C_S - k_C C_M}{k_C(C_M - C_S)}\right\}. \quad (14)$$

Furthermore, C_{max} can be estimated by substituting T_{max} into Eq. (10). We define this model as the Constant Surface area dissolution model (CS model).

2.2. The case in which surface area is not constant but changes with time

In the case of dissolution from a SD, the dissolution process may be accompanied by agglomeration between particles caused by the presence of polymers (Paudel et al., 2012; Adebisi et al., 2016). Therefore, it is not possible to entirely neglect the change in surface area caused by dissolution, even if an excess number of samples is added. We therefore developed a model that assumed part of dissolution rate constant k_D was variable.

We assume that at time $t = 0$, drugs do not form aggregates, that a final equilibrium exists between agglomerated and non-agglomerated drug, and that the surface area of the drug becomes constant. The initial surface area during dissolution is defined as S_0 and the final decreased and converged surface area is defined as S_{eq}. If the diminishing rate of surface area change is directly proportional to the surface area, which decreases as $\sigma(t) - S_{eq}$, the equation for the variable surface area $\sigma(t)$ is obtained as follows:

$$\frac{d\sigma(t)}{dt} = -k_E\left(\sigma(t) - S_{eq}\right), \tag{15}$$

where k_E represents the rate of decrease in the surface area of the drug. Solving Eq. (15) for $\sigma(t)$ gives

$$\sigma(t) = S_{eq} - \left(S_0 - S_{eq}\right)\exp\left(-k_E t\right). \tag{16}$$

Substituting Eq. (16) into Eq. (7) gives

$$\frac{dC_b}{dt} = \frac{k\left\{S_{eq} - \left(S_0 - S_{eq}\right)\exp\left(-k_E t\right)\right\}}{V}\left(C_{SL}(t) - C_b\right). \tag{17}$$

Converting the coefficients, $kS_{eq}/V = k_{eq}$, $kS_0/V = k_{D0}$ gives

$$\frac{dC_b}{dt} = \left\{k_{eq} - \left(k_{D0} - k_{eq}\right)\exp\left(-k_E t\right)\right\}\left(C_{SL}(t) - C_b\right), \tag{18}$$

where, k_{eq} is the dissolution rate constant when agglomeration reaches equilibrium and k_{D0} is the initial dissolution rate constant where aggregates do not exist. Incorporating Eq. (5) into Eq. (18) gives

$$\frac{dC_b}{dt} = \left\{k_{eq} - \left(k_{D0} - k_{eq}\right)\exp\left(-k_E t\right)\right\}\left\{C_S - \left(C_M - C_S\right)\exp\left(-k_C t\right) - C_b\right\}. \quad (19)$$

The equation describing the bulk concentration of the drug can be obtained by solving Eq. (19); however, it is impossible to solve this equation analytically. Therefore, in this study, a numerical method was applied to calculate C_b. We define this model as the Time-dependent Variable Surface area dissolution model (TVS model).

2.3. Calculation of the dissolution rate

The dissolution rate constant in the CS model, k_D, can calculated by a regression in Eq. (2) from the dissolution profile of stable crystals. In Eq. (1), assuming that the surface area of the drug is constant and $kS/V = k_D$ gives

$$\frac{dC_b}{dt} = k_D\left(C_S - C_b\right). \quad (20)$$

By solving Eq. (20) for C_b, the following equation is obtained:

$$C_b = C_S\left\{1 - \exp\left(-k_D t\right)\right\} \quad (21)$$

On the other hand, the initial dissolution rate constant in the TVS model, k_{D0}, can be calculated by a regression in the modified Noyes-Whitney Equation whose dissolution rate constant changes with time. Accordingly, it is assumed that k_D in Eq. (20) changes exponentially with time. If the constant describing the rate of decrease in the dissolution rate constant of stable crystals is k_{Dr} and the determinative dissolution rate constant of stable crystals is k_{Df}, Eq. (20) can be written as:

$$\frac{dC_b}{dt} = \left\{k_{Df} - \left(k_{D0} - k_{Df}\right)\exp\left(-k_{Dr} t\right)\right\}\left(C_S - C_b\right) \quad (22)$$

220 Solving Eq. (22) gives the bulk concentration C_b as follows:

221 $$C_b = C_S\left[1-\exp\left\{\frac{(k_{Df}-k_{D0})(1-\exp(-k_{Dr}t))}{k_{Dr}}-k_{Df}t\right\}\right] \quad (23)$$

222 By applying the non-linear least-squares method to Eq. (23) from the dissolution profile of

223 stable crystals, the initial dissolution rate constant of stable crystals k_{D0} can be obtained.

224

225

3. Materials and Methods

3.1. Materials

IB (Ibuprofen 25) and PVP (Kollidon® 25) was supplied by BASF Co., Ltd. (Tokyo, Japan).

3.2. Preparation of SD

SDs of IB/PVP were prepared using the solvent method. IB and PVP were mixed at different mass ratios (1:3, 1:5) and dissolved in ethanol. The solvent was evaporated and dried under reduced pressure overnight at room temperature. The dried product was ground using a mortar and pestle to prepare SD powders.

3.3. Powder X-ray Diffractometry (PXRD)

The solid properties of stable crystals of IB, PVP, SDs and the physical mixtures (PMs) were analyzed by PXRD using a Mini Flex II (Rigaku Corp., Tokyo, Japan) with Cu *K*α radiation, operated at an output voltage of 40 kV and an output current of 30 mA. The diffraction patterns with a 2θ range of 5–45° were recorded at a scanning rate of 5°/min.

3.4. Determination of the solubility of stable crystals, C_S

Two hundred milligrams of stable IB crystals were added into 50 mL of water and shaken at 37°C for 48 h. The supernatant was withdrawn and filtered through a 0.20μm membrane filter (Toyo Roshi Kaisha, Ltd., Tokyo, Japan) to remove the crystals. Each sample (50 μL) was diluted with 350 μL of a methanol:water 1:1 mixture, and the drug concentration of IB released into the medium was then quantitatively determined by reversed phase HPLC, LC-2010HC (Shimadzu, Kyoto, Japan) with a UV detector at 264 nm. The reversed phase HPLC column (Cadenza CD-18, 4.6 mm x150 mm, Imtakt, Japan) was

maintained at 40°C. The injection volume was 10 μL. The mobile phase consisted of 0.2% v/v formic acid in water and methanol (40:60, v/v) at a flow rate of 0.4 mL/min. The concentration of IB was quantified using the HPLC and the solubility was calculated from this concentration.

3.5. Determination of the dissolution rate constant, k_D and the initial dissolution rate constant, k_{D0}

The dissolution rate constant k_D and the initial dissolution rate constant k_{D0} were calculated from the dissolution behavior of stable IB crystals, using the paddle method listed in the Japanese Pharmacopoeia Seventeenth Edition (JP 17). The test solution was 900 or 500 mL of water at 37.0 ± 0.5°C and the paddle rotation speed was 100 rpm. IB (500 mg) from each batch was placed into the test solutions and 5 mL of the solutions were withdrawn and replaced with an equal volume of water. These samples were filtered, diluted and quantitated as described in *3.4*. Each rate constant was calculated by fitting the set of experimentally determined values to Eqs. (21) and (23), respectively.

3.6. Drug dissolution test of SDs

The dissolution behavior of the SDs was obtained by the dissolution test described in *3.5* using SDs as 500 mg of IB.

3.7. Curve fitting and analysis of dissolution test

The model equations were fitted to the results of dissolution tests by a nonlinear least-squares method using the statistics software package Origin® 9.1 (Originlab Corp., Northampton, MA) to calculate the parameters related to dissolution and their standard errors. Because this model was not able to be solved analytically, the model equations were solved

numerically. Explicit Runge-Kutta (4, 5) methods were used in numerical solutions and the Levenberg-Marquardt algorithm was used for nonlinear fitting. The simulation of estimated dissolution profiles and the calculation of the parameters, Y, C_{max} and T_{max} was carried out with a mesh size of $\Delta t = 0.1$ using the mathematical software Maple 2015 (Maplesoft, Waterloo, Canada).

3.8. Comparison of consistency between experimental data and curve obtained by mathematical models

Akaike's information criterion (AIC) (Neau et al., 1999), root mean square error (RMSE) and coefficient of determination (R^2) was used as a measure of goodness of fit of the experimental data to Eqs. (10) or (19). AIC and RMSE are respectively given by

$$\mathrm{AIC} = N \ln(\mathrm{RSS}) + 2P, \tag{24}$$

$$\mathrm{RMSE} = \sqrt{\frac{1}{N}\sum_{i=1}^{N}\left(y_i - \hat{y}_i\right)^2}, \tag{25}$$

$$\mathrm{R}^2 = 1 - \frac{\sum_{i=1}^{N}\left(y_i - \hat{y}_i\right)^2}{\sum_{i=1}^{N}\left(y_i - \bar{y}_i\right)^2}, \tag{26}$$

where N is the number of experimental data points, RSS is the residual sum of squares, P is the number of parameters, y_i is the measured value, $\hat{y}_i$ is the estimated value and $\bar{y}_i$ is the mean of measured values.

4. Results and discussion

4.1. Results of PXRD

Figure 3 shows the PXRD patterns for each sample; IB/PVP (1/5) SD (A), IB/PVP (1/5) physical mixture (PM) (B), IB/PVP (1/3) SD (C), IB/PVP (1/3) PM (D), PVP (E), and IB (F). Neither of the SD samples (A) and (C) showed diffraction peaks (a halo pattern), while diffraction peaks derived from IB were observed in both physical mixtures (B) and (D). Therefore, IB existed as an amorphous drug when preparing SDs, using PVP as a carrier.

4.2. Dissolution profiles of IB and estimation of dissolution rate

The solubility of a stable IB crystal in water at 37°C was found to be 80.0±6.5 μg/mL. **Figure 4** shows the dissolution profile for IB in 500 and 900 mL solvent volumes, respectively. IB concentration increased faster in 500 mL than that in 900 mL, suggesting that the drug promptly diffused through a small volume of the solvent, and this is consistent with the theory provided in the Noyes-Whitney Equation. In addition, theoretical values given by Eq. (23) fitted well with experimental values, unlike those given by Eq. (21). Overall, this suggests that the TVS model could better explain the dissolution behavior of stable crystals than the CS model when excess drug was added and the surface area of the drug was regarded as constant. **Table 1** shows the dissolution rate constant k_D and the initial dissolution rate constant k_{D0} of stable IB crystals that were calculated based on these results. A difference in dissolution rate constant was observed and the initial dissolution rate constant in the medium volume of 500 mL was approximately 1.7 times higher than that in 900 mL. From Eq. (20), the dissolution rate constant is calculated from the relationship between concentration and time. Since the concentration depends on the volume of the dissolution medium, it is conceivable that the dissolution rate based on the concentration varies depending on the medium volume. Therefore, when the dissolution rate constant is calculated

based on the dissolved mass, the rate constant based on dissolved mass can be calculated by k_D multiplied by the medium volume V from $k_D = kS/V$. When comparing with these values, they were 64.0 ± 2.5 mL/min at V = 500 mL and 54.9 ± 4.5 mL/min at V = 900 mL, which were almost similar. The dissolution rate constant is a constant depending on the diffusion coefficient, the thickness of the diffusion layer, and the surface area of drug, and it is considered that equivalent values were shown because these conditions were made identical. The using same calculation was performed for the initial dissolution rate constant k_{D0} in TVS model, and it was found that the values were 128 ± 11 mL/min at V = 500 mL and 138 ± 12 mL/min at V = 900 mL. From the above, it was shown that the dissolved mass per unit time was almost equal. The dissolution profile of the SDs was further fitted using the parameters related to dissolution rate constants.

4.3. Dissolution profiles of SD and parameter estimation with curve fitting

Figure 5 shows the dissolution profiles of SDs. Dashed curves represent the results for fitting using the CS model, and solid curves represent the results for fitting with the TVS model. Similar to the result for dissolution using only IB, IB concentration increased faster when using the smaller amount of dissolution medium. In addition, the SD with the high polymer ratio (IB/PVP (1/5)) showed faster dissolution and a higher concentration of the drug than the SD with a low polymer ratio (IB/PVP (1/3)). In addition, the fitted CS model was found not to account for the actual dissolution behavior under supersaturation conditions. On the other hand, the values estimated by the TVS model showed good agreement with experimental values during the early stage of dissolution and the supersaturation concentration of the drug gradually reached the solubility of the stable crystals. **Table 2** shows a quantitative evaluation of the differences between theoretical models, including AIC, RMSE, and R^2. The values of AIC and RMSE were low and that of

R^2 were high in the TVS model under all conditions, suggesting that the TVS model could explain the actual dissolution behavior of IB from the SDs more precisely than the CS model.

Table 3 shows the results analyzed by the TVS model and estimated parameters for the dissolution of the SD. The crystal precipitation rate constants from amorphous drug were increased as the polymer ratio and the amount of medium were increased. In addition, when the change per unit time with respect to the mass dissolved was taken into consideration similar to section 4.2, the crystal precipitation rate constant also increased as the medium volume increased. The bulk concentration of the drug in the vessel increased as the polymer ratio increased and the quantity of drug dispersed into the solution also increased. Therefore, stable crystals became easy to precipitate, and the precipitation rate was consequently increased. In addition, the concentration of the polymer in the vessel decreased as the medium volume was increased when the polymer ratio was constant because the quantity of PVP placed into the vessel was constant. On the other hand, the crystal generation from amorphous drug was disturbed by the crystal suppressant effect of the polymer in the solid dispersion and in the vessel (Alonzo et al., 2010). The crystal suppressant effect of the polymer became attenuated as the amount of the solvent increased. As a result, we concluded that the preparation of stable crystals became more rapid and the precipitation rate was high.

The potential solubility of the amorphous drug C_M was increased as the polymer ratio increased at medium volume of 500 mL. It was reported that the solubility of the SD using PVP was improved by increasing the polymer ratio (Najib et al., 1986; Newa et al., 2007; Jahangiri et al., 2015), suggesting that a higher polymer ratio in the SD could potentially allow the solubility to increase by this theory. On the other hand, the difference in the potential solubility associated with the polymer ratio was not recognized with a medium volume of 900 mL. Because an IB/PVP (1/3) SD in 900 mL showed a large estimated error

during fitting, it was thought that an accurate estimated value about the potential solubility C_M could not be obtained.

In this study, it was assumed that addition of excess drug to vessels allows the change in surface area to be neglected. Accordingly, a decreased rate constant of surface area change represents the agglomeration rate constant of SD at the time of exposure to the solvent. In addition, the equilibrium dissolution rate constant denotes the degree of agglomeration, and the rate decreases as the available surface area over which the drug directly contacts the solvent decreases. In other words, it is concluded that the agglomeration rate is fast when k_E is high, and that agglomeration of SD does not occur when k_{eq} is high. In both cases of medium volumes of 500 and 900 mL, the decrease rate constant k_E of IB/PVP (1/3) SD was approximately three times higher than that of IB/PVP (1/5) SD. From this, it was speculated that the SD with the lower polymer ratio aggregated faster when it was exposed to the solvent, and its available surface area became smaller. Furthermore, the equilibrium dissolution rate constant k_{eq} of IB/PVP (1/3) SD was also higher than IB/PVP (1/5). Thus, it was speculated that the eventual available surface area of the SD with the higher polymer ratio decreased considerably through agglomeration. Because the quantity of IB was integrated for each experimental system in this study, the quantity and concentration of polymer in the vessel became larger as the polymer ratio of the SD increased. Therefore, it is suggested that the SD with the larger polymer ratio had the greater interaction between the SD and the polymer, so its available surface area was smaller than that with a smaller polymer ratio as a result of agglomeration leading to larger particle diameters.

4.4. Estimation of secondary parameters and discussion

Table 4 (A) shows the maximum concentration of the drug and the time required to reach the maximum concentration, estimated from the measured values. C_{max} increased with

increasing polymer ratio in a medium volume of 500 mL, and T_{max} was prolonged as that the quantity of solvent increased. A higher C_{max} was observed because the amorphous drug C_M increased as the polymer ratio was increased and the concentration of IB rose prior to the precipitation of the stable crystals. In addition, because the equilibrium dissolution rate constant of the drug decreased when the volume of a solvent increased, an increase in T_{max} was observed. **Table 4 (B)** shows the secondary parameters for dissolution, Y, C_{max}, T_{max}, estimated by curve fitting. The maximum concentration of the drug C_{max} estimated from the theoretical values showed good agreement with C_{max} calculated from the measured values and the relative error in C_{max} between the estimated and measured values was calculated as around 5% at most. Although the relative errors in T_{max} increased generally, no significant difference between estimated and measured values was apparent. Therefore, we conclude that C_{max} and T_{max} estimated using this mathematical model accurately reflect the values for the actual dissolution behavior of the drug. The precision of these parameters can be improved by sampling more closely at the peak of supersaturation. The increment of dissolution Y reached a high value as the polymer ratio increased and showed a value of approximately four times when comparing IB/PVP (1/3) SD and IB/PVP (1/5) SD in a medium volume of 500 mL. The increase in polymer ratio not only caused a large precipitation ratio of stable crystals, but also kept the dissolution rate constant and concentration high. Therefore, the contribution to the increase in the concentration of the drug through dissolution was larger than the decrease in the concentration of the drug through precipitation. As a result, we suggest that supersaturation was maintained for a long period by the high concentration when the polymer ratio was large. In contrast, Y was smaller when there was a large solvent volume because the contribution of the increase in drug concentration with dissolution was smaller, and the drug concentration was lower in comparison with the case of a small solvent volume. Thus, using the increment of the dissolution Y, it is possible to quantitatively analyze supersaturation

under the conditions of constant solvent volume, to evaluate the solubility of different SD samples.

5. Conclusions

In this study, a novel mathematical model representing drug dissolution at the solid-liquid interface was developed, and its verification was evaluated for a SD of IB/PVP. This model was fitted to the dissolution profile of the SD, and the estimated values from this model showed good agreement with experimental values, indicating that the model could describe the dissolution profile of the SD. In addition, this model could estimate the potential solubility of the drug in the SD and the increment of dissolution Y was shown to be a useful index that indicates the degree of drug dissolution of a preparation. If the drug dissolves without agglomeration, it is thought that the simpler CS model can be applied to drug dissolution. However, since the dissolution of SDs often proceeds with agglomeration, the TVS model assuming that the available surface area changed during dissolution is more appropriate to the analysis of supersaturation of SDs. This model would be difficult to predict their dissolution behaviors because this should be performed by using numerical analysis. However, only just two physicochemical parameters (solubility and dissolution rate constant) obtained by other independent experiments are needed, suggesting that this model would be applicable for analyzing dissolution behavior of other solid dispersion formulations.

REFERENCES

Adebisi, A. O., Kaialy, W., Hussain, T., Al-Hamidi, H., Nokhodchi, A., Conway, B. R., Asare-Addo, K., 2016, Solid-state, triboelectrostatic and dissolution characteristics of spray-dried piroxicam-glucosamine solid dispersions. Colloids Surf., B. 146, 841–851.

Alonzo, D. E., Zhang, G. G., Zhou, D., Gao, Y., Taylor, L. S., 2010, Understanding the behavior of amorphous pharmaceutical systems during dissolution. Pharm. Res. 27, 608–618.

Chen, W., Desai, D., Good, D., Timmins, P., Paruchuri, S., Wang, J., Ha, K., 2016, Mathematical model-based accelerated development of extended-release metformin hydrochloride tablet formulation. AAPS PharmSciTech. 17, 1007–1013.

Childs, S. L., Kandi, P., Lingireddy, S. R., 2013, Formulation of a danazol cocrystal with controlled supersaturation plays an essential role in improving bioavailability. Mol. Pharmaceutics. 10, 3112–3127.

Dokoumetzidis, A., Macheras, P., 2006, A century of dissolution research: from Noyes and Whitney to the Biopharmaceutics Classification System. Int. J. Pharm. 321, 1–11.

Douroumis, D., Fahr, A., 2006, Nano- and micro-particulate formulations of poorly water-soluble drugs by using a novel optimized technique. Eur. J. Pharm. Biopharm. 63, 173–175.

Dukeck, R., Sieger, P., Karmwar, P., 2013, Investigation and correlation of physical stability, dissolution behavior and interaction parameter of amorphous solid dispersions of telmisartan: A drug development perspective. Eur. J. Pharm. Sci. 49, 723–731.

Gao, J. Y., 2012, Studying Dissolution with a Model Integrating Solid-Liquid Interface Kinetics and Diffusion Kinetics. Anal. Chem. 84, 10671–10678.

Jackson, J. J., Kestur, U. S., Hussain, M. A., Taylor, L. S., 2016, Dissolution of danazol amorphous solid dispersions: Supersaturation and phase behavior as a function of drug loading and polymer type. Mol. Pharmaceutics. 13, 223–231.

462 Jahangiri, A., Barzegar-Jalali, M., Garjani, A., Javadzadeh, Y., Hamishehkar, H., Afroozian,
463 A., Adibkia, K., 2015, Pharmacological and histological examination of atorvastatin-
464 PVP K30 solid dispersions. Powder Technol. 286, 538–545.

465 Jakubiak, P., Wagner, B., Grimm, H. P., Petrig-Schaffland, J., Schuler, F., Alvarez, R., 2016,
466 Development of a unified dissolution and precipitation model and its use for the
467 prediction of oral drug absorption. Mol. Pharmaceutics. 13, 586–598.

468 Kawabata, Y., Wada, K., Nakatani, M., Yamada, S., Onoue, S., 2011. Formulation design for
469 poorly water-soluble drugs based on biopharmaceutics classification system: Basic
470 approaches and practical applications. Int. J. Pharm. 420, 1–10.

471 Knopp, M. M., Chourak, N., Khan, F., Wendelboe, J., Kangguth, P., Rades, T., Holm, R.,
472 2016, Effect of polymer type and drug on the in vitro and in vivo behavior of amorphous
473 solid dispersions. Eur. J. Pharm. Sci. 105, 106–114.

474 Knopp, M. M., Nguyen, J. H., Becker, C., Francke, N. M., Jørgensen, E. B. Holm, P., Holm,
475 R., Mu, H., Rades, T., Langguth, P., 2016, Influence of polymer molecular weight on in
476 vitro dissolution behavior and in vivo performance of celecoxib:PVP amorphous solid
477 dispersions. Eur. J. Pharm. Biopharm. 101, 145–151.

478 Laaksonen, T., Aaltonen, J., 2013, Modeling solid-state transformations occurring in
479 dissolution testing. Int. J. Pharm. 447, 218–223.

480 Mah, P. T., Peltonen, L., Novakovic, D., Rades, T., Strachan, C. J., Laaksonen, T., 2016, The
481 effect of surfactants on the dissolution behavior of amorphous formulations. Eur. J.
482 Pharm. Biopharm. 103, 13–22.

483 Makwana, V., Jain, R., Patel, K., Nivsarkar, M., Joshi, A., 2015, Solid lipid nanoparticles
484 (SLN) of Efavirenz as lymph targeting drug delivery system: Elucidation of mechanism
485 of uptake using chylomicron flow blocking approach. Int. J. Pharm. 495, 439–446.

486 Mishra, D. K., Dhote, V., Bhargava, A., Jain, D. K., Mishra, P. K., 2015, Amorphous solid
487 dispersion technique for improved drug delivery: basics to clinical applications. Drug
488 Delivery Transl. Res. 5, 552–565.

Najib, N. M., Suleiman, M., Malakh, A., 1986, Characteristics of the in vitro release of ibuprofen from polyvinylpyrrolidone solid dispersions. Int. J. Pharm. 32, 229–236.

Neau, S. H., Howard, M. A., Claudius, J. S., Howard, D. R., 1999, The effect of the aqueous solubility of xanthine derivatives on the release mechanism from ethylcellulose matrix tablets. Int. J. Phram. 179, 97–105.

Newa, M., Bhandari, K. H., Li, D. X., Kwon, T., Kim, J. A., Yoo, B. K., Woo, J. S., Lyoo, W. S., Yong, C. S., Choi, H. G., 2007, Preparation, characterization and in vivo evaluation of ibuprofen binary solid dispersions with poloxamer 188. Int. J. Pharm. 343, 228–237.

Nielsen, L., Rades, T., Müllertz, A., 2015, Stabilisation of amorphous furosemide increases the oral drug bioavailability in rats. Int. J. Pharm. 490, 334–340.

Noyes, A. A., Whitney, W. R., 1897, The rate of solution of solid substances in their own solutions, J. Am. Chem. Soc. 19, 930–934.

Ozaki, S., Kushida, I., Yamashita, T., Hasebe, T, Shirai, O., Kano, K., 2013, Inhibition of crystal nucleation and growth by water-soluble polymers and its impact on the supersaturation profiles of amorphous drugs. J. Pharm. Sci. 102, 2273–2281.

Paaver, U., Lust, A., Mirza, S., Rantanen, J., Veski, P., Heinämäki, J., Kogermann, K., 2012, Insight into the solubility and dissolution behavior of piroxicam anhydrate and monohydrate forms. Int. J. Pharm. 431, 111–119.

Paudel, A., Nies, E., Mooter, G. V., 2012, Relating hydrogen-bonding interactions with the phase behavior of naproxen/PVP K 25 solid dispersions: Evaluation of solution-cast and quench-cooled films. Mol. Pharmaceutics. 9, 3301–3317.

Raimi-Abraham, B. T., Mahalingam, S., Davies, P. J., Edirisinghe, M., Craig, D. Q. M., 2015, Development and Characterization of Amorphous Nanofiber Drug Dispersions Prepared Using Pressurized Gyration. Mol. Pharmaceutics. 12, 3851–3861.

Sanphui, P., Devi, V. K., Clara, D., Malviya, N., Ganguly, S., Desiraju, G. R., 2015, Cocrystals of hydrochlorothiazide: Solubility and diffusion/ permeability enhancements through drug–coformer interactions. Mol. Pharmaceutics. 12, 1615–1622.

516 Sarode, A. L., Sandhu, H., Shah, N., Malick, W., Zia, H., 2013, Hot melt extrusion (HME)
517 for amorphous solid dispersions: Predictive tools for processing and impact of drug-
518 polymer interactions on supersaturation. Eur. J. Pharm. Sci. 48, 371–384.

519 Sarode, A. L., Wang, P., Obara, S., Worthen, D. R., 2014, Supersaturation, nucleation, and
520 crystal growth during single- and biophasic dissolution of amorphous solid dispersions:
521 Polymer effects and implications for oral bioavailability enhancement of poorly water
522 soluble drugs. Eur. J. Pharm. Biophgarm. 86, 351–360.

523 Sugano, K., 2011, Fraction of a dose absorbed estimation for structurally diverse low
524 solubility compounds. Int. J. Pharm. 405, 79–89.

525 Sun, D. D., Lee, P. I., 2013, Evolution of supersaturation of amorphous pharmaceuticals: the
526 effect of rate of supersaturation generation. Mol. Pharmaceutics. 10, 4330–4346.

527 Tsinman, K., Avdeef, A., Tsinman, O., Voloboy, D., 2009, Powder dissolution method for
528 estimating rotating disk intrinsic dissolution rates of low solubility drugs. Pharm. Res.
529 26, 2093–2100.

530 Tsume, Y., Takeuchi, S., Matsui, K, Amidon, G. E., Amidon, G. L., 2015, In vitro dissolution
531 methodology, mini-Gastrointestinal Simulator (mGIS), predicts better in vivo
532 dissolution of a week base drug, dasatinib. Eur. J. Pharm. Sci. 76, 203–212.

533 Wlodarski, K., Sawicki, W., Haber, K., Knapik, J., Wojnarowska, Z., Paluch, M., Lepek, P.,
534 Hawelek, L., Tajber, L., 2015, Physicochemical properties of tadalafil solid dispersions
535 – Impact of polymer on the apparent solubility and dissolution rate of tadalafil. Eur. J.
536 Pharm. Biopharm. 94, 106–115.

537 Zhang, P., Torre, T. Z. G., Welch, k., Bergström, Strømmea, M., 2016, Supersaturation of
538 poorly soluble drugs induced by mesoporous magnesium carbonate. Eur. J. Pharm. Sci.,
539 93, 468–474.

540

TABLES

Table 1. Estimated values of parameters related to the dissolution of stable crystals, k_D, k_{D0}, k_{Df} and k_{Dr}, at medium volumes of 500 and 900 mL. Each parameter is the mean value ± S. E. (n=3)

Volume (mL)	CS model	TVS model		
	Dissolution rate constant k_D (min^{-1})	Initial dissolution rate constant k_{D0} (min^{-1})	Constant k_{Df} (min^{-1})	Constant k_{Dr} (min^{-1})
500	0.128 ± 0.005	0.256 ± 0.022	0.059 ± 0.009	0.413 ± 0.153
900	0.061 ± 0.005	0.153 ± 0.013	0.034 ± 0.005	0.294 ± 0.045

Table 2. Estimated AIC, RMSE and coefficient of determination (R^2) values for the CS and TVS models at medium volumes of 500 and 900 mL.

IB/PVP	Volume (mL)	CS model			TVS model		
		AIC	RMSE	R^2	AIC	RMSE	R^2
1/3	500	144	8.17	0.904	116	3.95	0.971
	900	124	7.36	0.939	94	3.01	0.986
1/5	500	158	11.99	0.678	90	4.66	0.938
	900	151	10.06	0.813	122	1.96	0.991

Table 3. Estimated values of parameters related to dissolution of SD, k_C, C_M, k_E and k_{eq}, at medium volumes of 500 and 900 mL. Each parameter is the mean value ± S. E. (n=3)

IB/PVP	Volume (mL)	k_C (min^{-1})	C_M (μg/mL)	k_E (min^{-1})	k_{eq} (min^{-1})
1/3	500	$3.09 \pm 1.03 \times 10^{-3}$	$1.02 \pm 0.05 \times 10^{2}$	1.53 ± 0.48	$2.54 \pm 0.09 \times 10^{-2}$
	900	$6.36 \pm 1.52 \times 10^{-3}$	$1.37 \pm 0.22 \times 10^{2}$	1.75 ± 0.20	$1.22 \pm 0.02 \times 10^{-2}$
1/5	500	$5.09 \pm 1.02 \times 10^{-3}$	$1.63 \pm 0.20 \times 10^{2}$	$5.61 \pm 1.22 \times 10^{-1}$	$1.88 \pm 0.04 \times 10^{-2}$
	900	$6.37 \pm 1.53 \times 10^{-3}$	$1.38 \pm 0.16 \times 10^{2}$	$6.32 \pm 1.83 \times 10^{-1}$	$1.12 \pm 0.15 \times 10^{-2}$

Table 4. (A) Measured (B) and estimated values of secondary parameters related to dissolution of SD, Y, C_{max} and T_{max}, at 500 and 900 mL. Y was calculated only in the case of estimated values. Each estimated parameter is the mean value ± S. E. (n=3)

(A)

IB/PVP	Volume (mL)	C_{max} (μg/mL)	T_{max} (min)
1/3	500	98.6	150
	900	95.5	180
1/5	500	129.7	120
	900	96.4	150

(B)

IB/PVP	Volume (mL)	C_{max} (μg/mL)	T_{max} (min)	Y (μg/mL·min)
1/3	500	93.6 ±1.7	155 ±11	$3.58 \pm 0.33 \times 10^3$
	900	93.7 ±2.4	206 ±11	$2.96 \pm 0.73 \times 10^3$
1/5	500	124 ±3	113 ±7	$1.32 \pm 0.64 \times 10^4$
	900	99.7 ±3.4	191 ±2	$6.17 \pm 1.11 \times 10^3$

FIGURES

Figure 1. Dissolution from solid drug: (A) the stable crystal; (B) the metastable crystal or amorphous drug with a reaction at the solid-liquid interface upon dissolution.

Figure 2. Estimated dissolution profile of the drug: (A) the stable crystal; (B) the metastable crystal or amorphous drug with a reaction at the solid-liquid interface upon dissolution.

Figure 3. Powder X-ray Diffractometry patterns of (A) IB/PVP (1/5) solid dispersion (SD), (B) IB/PVP (1/5) physical mixture (PM), (C) IB/PVP (1/3) SD, (D) IB/PVP (1/3) PM, (E) PVP and (F) IB.

Figure 4. Experiments and simulations of dissolution profiles of IB with different medium volumes: (A) 500 mL; (B) 900 mL.

Symbols: experimental values ± S. D. (n=3); solid curves: Eq. (21); and dashed curves: Eq. (23).

Figure 5. Experiments and simulations of dissolution profiles of solid dispersion (SD) with various polymer ratios and bulk volumes: (A) IB/PVP (1/3) SD, V=500 mL, (B) IB/PVP (1/3) SD, V=900 mL, (C) IB/PVP (1/5) SD, V=500 mL, (D) IB/PVP (1/5) SD, V=900 mL.

Symbols: experimental values ± S. D. (n=3); dashed curves: Eq. (10); and solid curves: Numerical solutions of Eq. (19).

Figure 1. **Hirai *et al.***

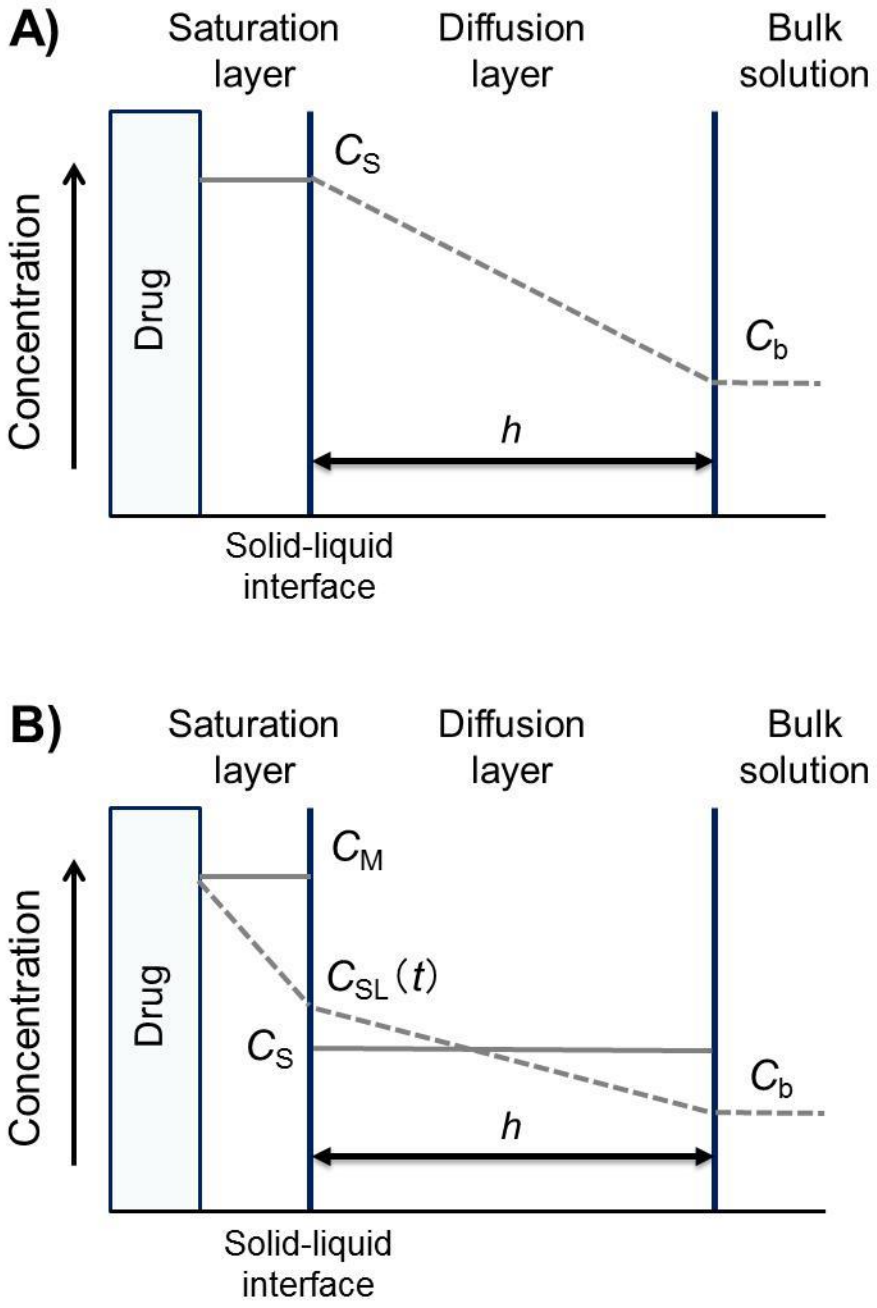

585

586

587

588

Figure 2. **Hirai *et al.***

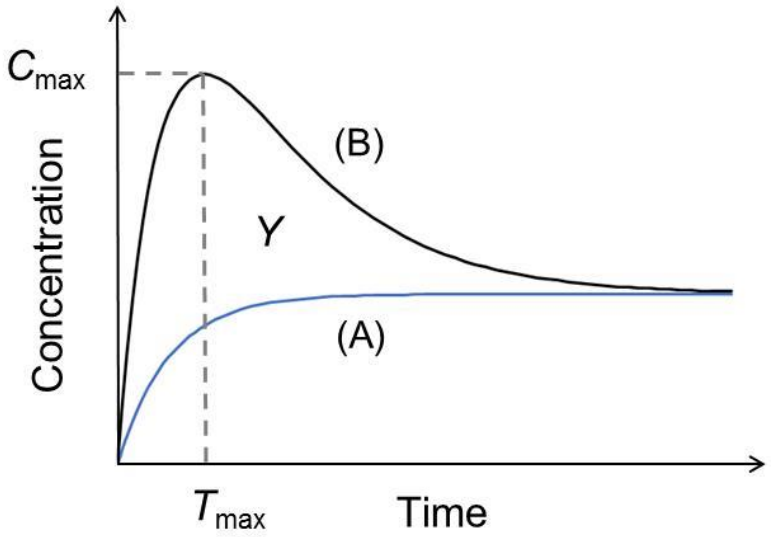

589

Figure 3. **Hirai *et al.***

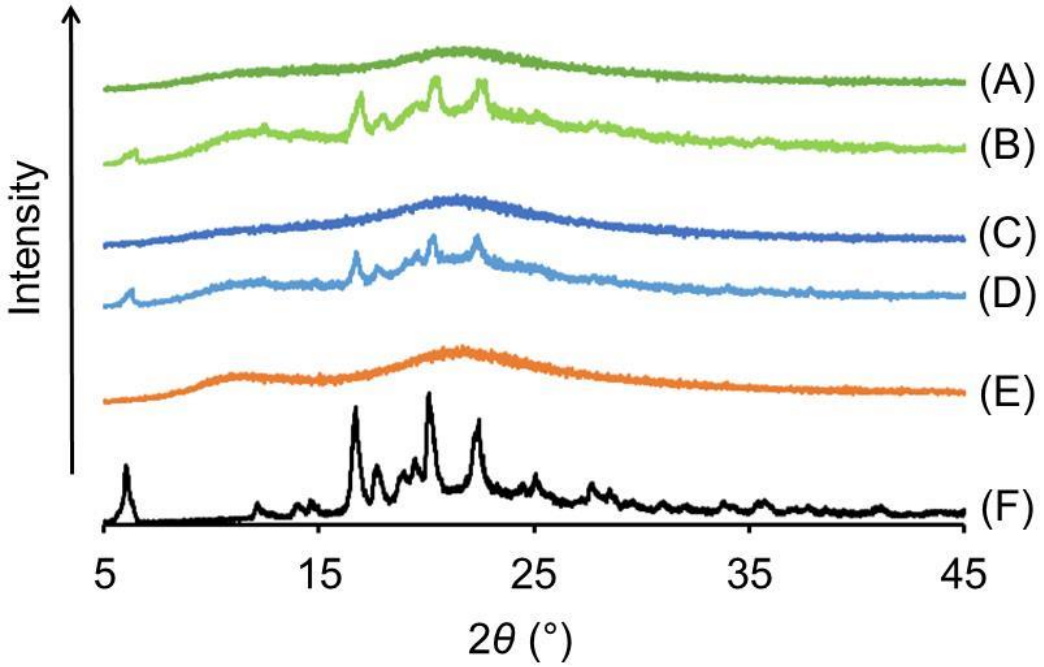

590

591

592

593

Figure 4. **Hirai *et al.***

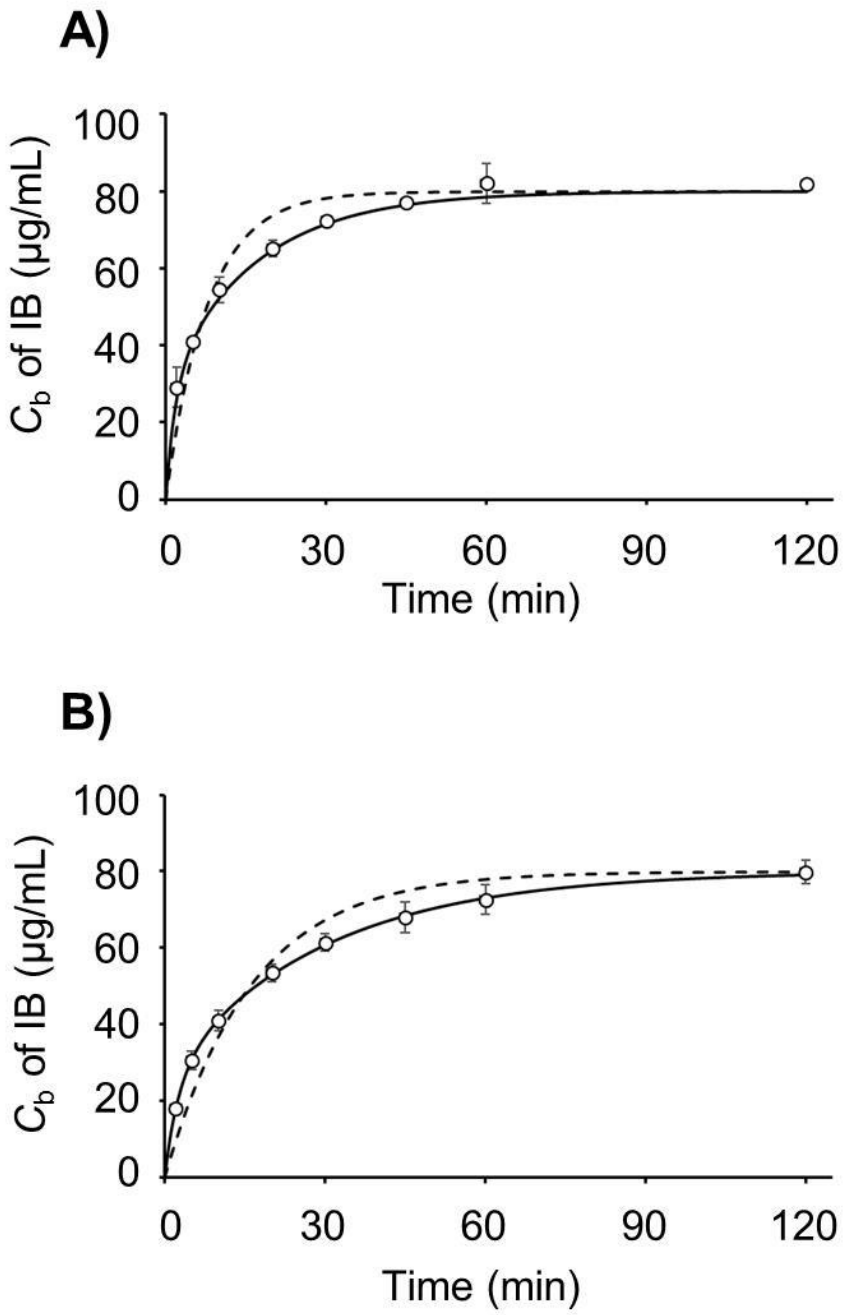

Figure 5.

Hirai *et al.*

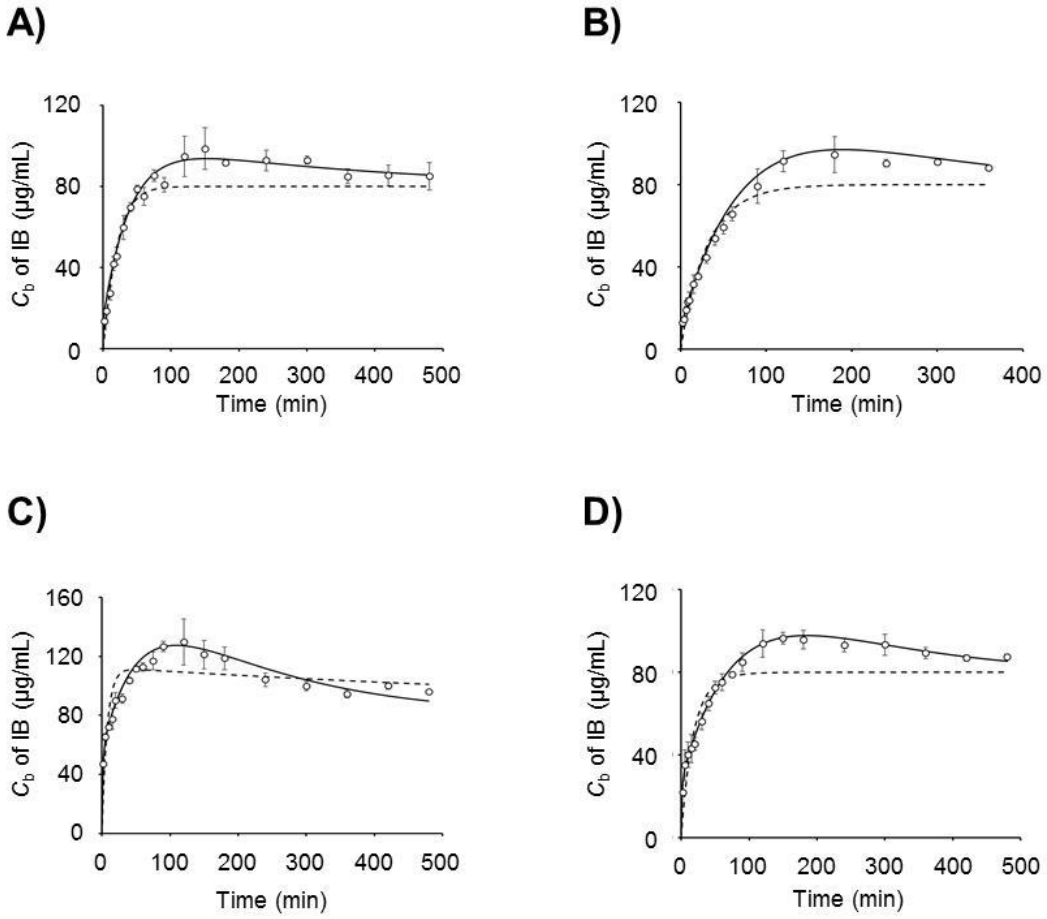

598

599